Article

Substitution Effects on the Reactivity and Thermostability of Five-Membered Ring Fluorides

Tongyun Zhang, Chengping Zhang, Xiaoxun Ma,* and Hengdao Quan*

| Read Online

ACCESS | 📊 Metrics & More | 📖 Article Recommendations | 📑 Supporting Information

ABSTRACT: Recently, five-membered ring fluorides (c-C$_5$Fs) have been significantly desirable in green chlorofluorocarbon substitutes due to their practically flexible application in various fields and environmental friendliness. Detailed knowledge regarding different substitution effects on their environmental properties and thermal stability is very limited due to their high-cost experiments. Here, comprehensive density functional theory and ab initio molecular dynamics calculations were performed to explore the relative electrophilic and nucleophilic reactivity and thermostability of c-C$_5$F chemicals. The electronic properties induced by substitution effects of c-C$_5$Fs were first explored. The environmental friendliness of c-C$_5$Fs including 1,1,2,2,3,3-hexafluorocyclopentane (F6A), 1,1,2,2,3,3,4-heptafluorocyclopentane (F7A), cis-1,1,2,2,3,3,4,5-octafluorocyclopentane (F8A), 3,3,4,4,5,5-hexafluorocyclopentene (F6E), 1,3,3,4,4,5,5-heptafluorocyclopentene (F7E), octafluorocyclopentene (F8E), 1-chloro-3,3,4,4,5,5-hexafluorocyclopent-1-ene (F6-1), and 1-chloro-2,3,3,4,4,5,5-heptafluorocyclopent-1-ene (F7-1) was validly confirmed. Besides, their thermal stabilities at 600 K temperature were concluded due to their flexible carbon skeletons, where both in-plane stability and slight aromaticity of F6E were in peculiar found to contribute substantially. We also would like to stress the future application of F6-1 due to its significant out-plane stability. This study may pave the way for the development of chlorofluorocarbon substitutes.
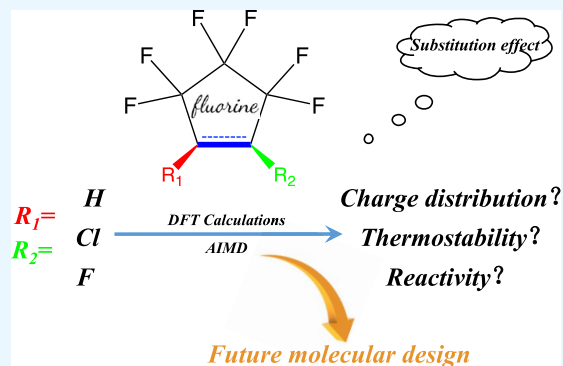
1. INTRODUCTION

Currently, freon (chlorofluorocarbons, CFCs) has been identified as the main culprit of ozone depletion. From this point of view, to address the global environmental challenges of the Antarctic ozone hole and global warming, three generations of CFC substitutes have been developed to diminish the value of ozone-depleting potential and global warming potential (GWP) of fluorinated substances.[1] The three generation compounds are normally composed of hydrochlorofluorocarbons, hydrofluorocarbons (HFCs), hydrofluoroethers, and hydrofluoroolefins (HFOs), which have many significant applications in foaming agents, aerosols, solvents, refrigerants, and heat transfer fluids. In addition to aliphatic substitutes, cyclic fluorides have also attracted growing interests as novel alternatives.

Five-membered ring fluorides (c-C$_5$Fs), including cyclic HFCs (c-HFCs) and HFOs (c-HFOs), are receiving great popularity in cleaning, etching, heat transfer fluids, and so on and becoming the hot spot in the research field of CFC substitutes. 1,1,2,2,3,3-Hexafluorocyclopentane (F6A),[2] 1,1,2,2,3,3,4-heptafluorocyclopentane (F7A),[3,4] and cis-1,1,2,2,3,3,4,5-octafluorocyclopentane (cis-F8A, hereinafter abbreviated as F8A)[5] have been revealed as novel and promising cleaning agents.[6] Other important broad classes of the utilization of F7A are extinguishants,[7] cleaning photosensitive fuel,[8] and solvents commonly used in the preparation

of polymer membrane fuel cells,[9] lithium batteries,[10] etc. 3,3,4,4,5,5-Hexafluorocyclopentene (F6E) and 1,3,3,4,4,5,5-heptafluorocyclopentene (F7E) have been widely used as heat pump fluids,[11−13] etching agents, and important industrial intermediate materials.[14,15] For octafluorocyclopentene (F8E), its polymer film deposition rate and etch selective ratio of SiO$_2$ were already proved to be better than those of currently popular c-C$_4$F$_8$.[16−18] More recently, for electronic fluorinated liquids including immersion coolants, a series of halogenated (fluorine or chlorine) cyclic olefins have been extensively used as convenient raw materials to produce cyclic fluorinated ethers and unsaturated perfluoramines.[19,20] Beyond these, since chlorine-containing HCFOs like HCFO-1233zd(Z) are well applicable in cleaning,[21] we would also like to suggest the potential application of washing agents, raw materials, and solvents of 1-chloro-3,3,4,4,5,5-hexafluorocyclopent-1-ene (F6-1), 1,2-dichloro-3,3,4,4,5,5-hexafluorocyclopent-1-ene (F6-12),
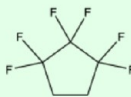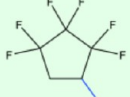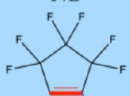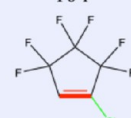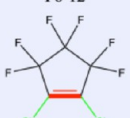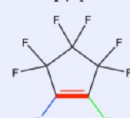
Scheme 1. Investigated Five-Membered Ring Fluorides in This Work

and 1-chloro-2,3,3,4,4,5,5-heptafluorocyclopent-1-ene (F7-1) (Scheme 1).

As far, for fluorine chemicals, substantial efforts have been made to study the synthetic routes of c-C_5Fs. To produce F7A, F7-1 was reacted with hydrogen in the presence of a Pd-based catalyst (yield >90%), where byproducts including F7E and F6A were found.[22,23] Subsequently, F6E was effectively prepared by F7A in solvents of DMF or DMAC, and F7E could be obtained from F8A by similar dehydrofluorination as well. However, no elimination occurred in F6A possibly due to its extremely weak acidity as fluorine was introduced.[24] F7-1 and F8E were reported to be obtained from the selective fluorination of F6-12 and 1,4-dichlorohexafluorocyclopentene (F6-14), the yield of which reached up to 78.8 and 32.5%, respectively.[25] On the other hand, as a facile raw material, F6-12 could produce F6-1 with zinc in DMF (yield = 76.4%) or DMAC (yield = 84.3%), while, in contrast, F7-1 was able to selectively generate F7E (yield up to 5.8%) and F6-1 by hydrodehalogenation. It was suggested that hydrodehalogenation of such perchlorofluorocycloolefin would rather occur on the C(sp^2) position than localize on the C(sp^3) position.[26] Over PAF-supported metal catalysts, especially for Pd and Pt, F6-12 produced F6A with high yield more than 90%. With similar fate, F8E underwent an hydrodefluorination to produce cis-F8A.[24] For F6-12, in DMF with AlCl$_3$, it could be obtained from F8E and F7-1 through Cl−F exchange reaction, the yields of which reached 86.8 and 87.5%, respectively.[27]

Nevertheless, before an industrial-scale application, the attractive properties of c-C_5Fs give us desire of worthily persistent exploration of their environmental performances including the 100-year global warming potential (GWP$_{100}$). In this regard, Guo et al.[28] reported the rate constant (k_{rate}) of F6A to be $2.94 \pm 0.05 \times 10^{-13}$ s^{-1}(molec/cm^3)$^{-1}$ through a relative experiment method, GWP$_{100}$ of which was 107. Similarly, Zhang et al.[29] explored the GWP$_{100}$ of F7A and cis-F8A to be 211 and 241, respectively. By adopting a C=C bond, the k_{rate} values of F6E,[30] F7E,[31] and F8E[32] were reported to be 1.08 ± 0.04, 5.20 ± 0.09, and 1.01 ± 0.16 s^{-1}(molec/

cm^3)$^{-1}$, respectively, the GWP$_{100}$ values of which were 15, 42, and 28, respectively. These illustrate the negligible atmospheric impact of such c-C_5Fs, but unfortunately, there is still a lack of relevant investigations on F6-1, F6-12, and F7-1.

Excluding the environmental performance, another key factor decisive to substances' application is the thermal stability, which is commonly required under severe and strict working conditions. A temperature higher than 150 °C even 200 °C of the working medium fluids in high-temperature heat source machine is usually recommended.[13] Often the limited high etch temperatures are, to our knowledge, about 85 °C.[33] For F7A, the thermolysis temperature was reported to be 580 °C, which is significantly affected by increasing temperatures.[7] From an experimental respective, F6E decomposes after 650 °C, while F7E and F8E remain stable at 700 °C. These facts made it a significant investigation to study the role of potential thermostability.[34]

However, since the above studies are sporadic, deeper knowledge related to the reactivity, atmospheric chemical properties, and thermal stability of these substances is still confusing. Theoretical calculations have become a very reliable tool to explore the molecular characteristics and reveal the nature at the electronic level. Thus, here, comprehensive density functional theoretical calculations and ab initio molecular dynamics (AIMD) simulations were conducted to understand the reactivity and thermal stability of the above c-C_5Fs. The current work focused on the effects of substitution from H, F, and Cl atoms and the C=C bond by employing analyses including bond character, electrostatic and van der Waals (vdW) interaction characteristics, and electron delocalization. To our knowledge, this is the first work to systematically report the substitution effects on atmospheric chemical properties and thermal stability. Although issues, such as deviation between the calculated atmosphere lifetime with experiment data of F7A, still need to be addressed by further fine experimental and theoretical design, this work proved the replacement of c-C_5F chemicals as a resultful strategy to support the upgrading of CFC substitutes.
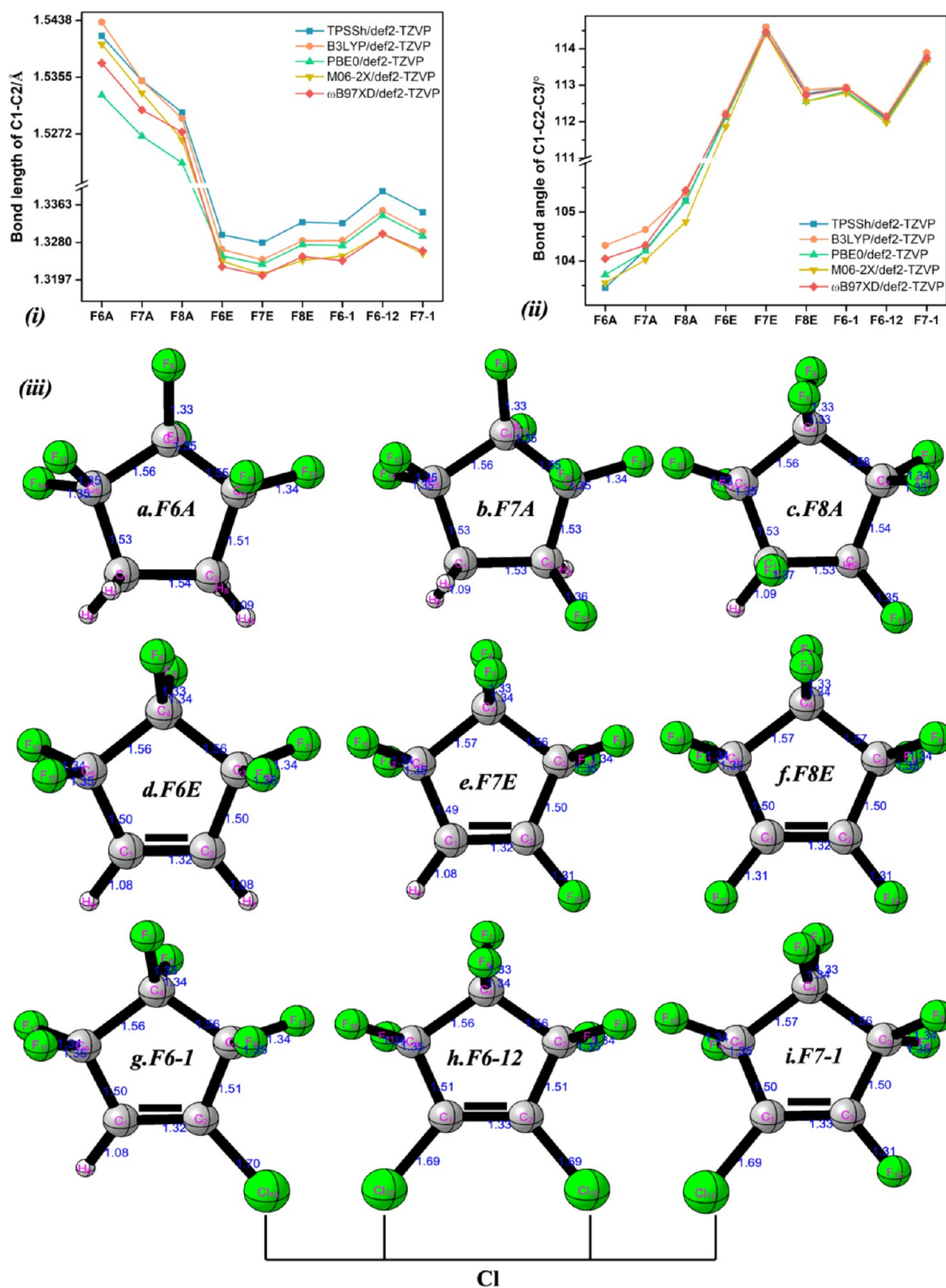
Figure 1. (i) C1−C2 bond lengths calculated at various methods; (ii) bond angles of C1−C2−C3 at various calculation methods; (iii) optimized geometries at the ωB97XD/def2-TZVP level.

2. THEORETICAL METHODS

All quantum chemistry calculations presented in this work were performed by using the Gaussian 16 program (C.01).[35] Unless otherwise mentioned, all results were computed by adopting the ωB97XD exchange−correlation functional[36] in conjunction with the def2-TZVP basis set[37] in the gas phase. Frequency calculations were operated to determine whether each stationary point was a stable or a transitional structure. For the atmospheric degrading processes of c-C_5Fs initiated by OH radicals, intrinsic reaction coordinate calculations for typical transition states were computed to confirm the reaction pathways and to identify intermediates.[38] In order to obtain relative energies for the species involved in the atmospheric degradation, the ωB97M-V functional[39] in combination with a very large def2-QZVP basis set[37] was employed in single-point
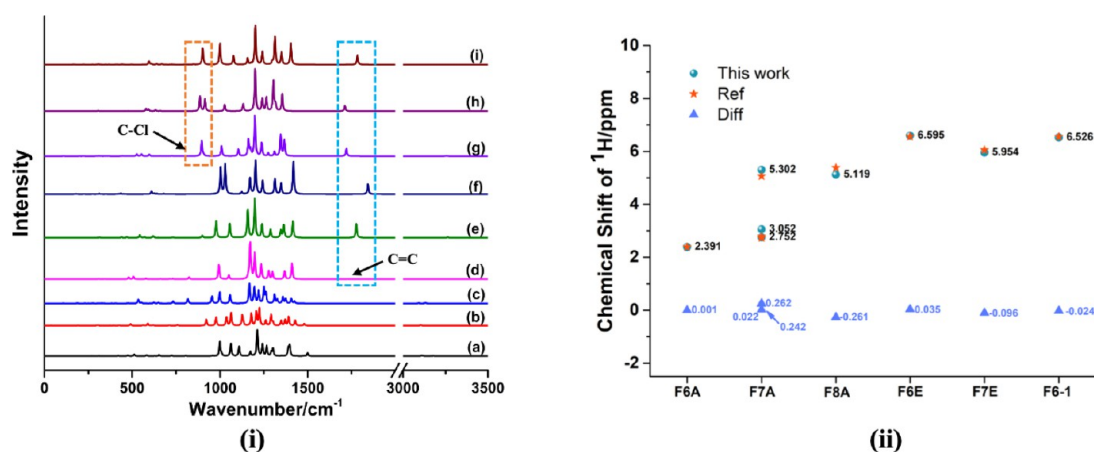
Figure 2. IR (i) and ^{1}H NMR (ii) spectra of (a) F6A, (b) F7A, (c) F8A, (d) F6E, (e) F7E, (f) F8E, (g) F6-1, (h) F6-12, and (i) F7-1. The ^{1}H NMR results of F8A and F6-12 were referred to refs 23, 26, respectively, and data of others were referred to ref 62.

calculations by using the ORCA program.[40] All energy data were processed with the help of the Shermo program (version 2.3),[41] where zero-point energies were considered with ZPE scale factors (0.985 for the ωB97XD method).[42]

To investigate the dynamic behavior, AIMD simulations were performed through the ORCA program using the r2SCAN-3c method.[43] A step size of 0.5 fs was adapted, in which a CSVR thermostat was employed for a constant temperature. The beginning atomic velocities were imparted randomly based on Boltzmann−Maxwell distribution. Anisotropy of the current-induced density (ACID) analysis[44] was achieved through the ACID code based on the output file of Gaussian 16 and finally generated plots via POV-Ray rendering.[45] Other physical and chemical analyses were all performed by the Multiwfn 3.8 program.[46] The isosurface maps of various orbitals and real-space functions were rendered by means of Visual Molecular Dynamics software[47] based on the output files from Multiwfn.

3. RESULTS AND DISCUSSION

3.1. Calibration of the Computational Strategy and Structures. A correct geometry is the premise and guarantee for accurate computations and exploration of various molecular characteristics. Consequently, in this work, we started with the calibration of calculation strategies to identify combinations of functionals and basis sets that could correctly reflect the structural properties of c-C$_5$F compounds. Though some structural parameters have been revealed in previous work,[7,48−50] there are a lack of the experimental observation and the computational strategy calibration to guarantee for the accurate exploration of their molecular properties. In this paper, the very commonly used TPSSh,[51] B3LYP,[52,53] PBE0,[54] M06-2X,[55] and ωB97XD functionals[56,57] were adopted in conjunction with the def2-TZVP basis set. We noted that, in all cases, the optimized geometries were exactly nonplanar at equilibrium (see in Figure S1) and belonged to the C1 point group. Figure 1(i),(ii) shows the calibration based on their bond lengths of C1−C2 and bond angles of C1−C2−C3, respectively, which were measured at various theoretical levels. The C1−C2 bond length estimated by TPSSh or PBE0 functionals appeared to be abnormal for alkenes or olefins. M06-2X functionals were likely to provide inconsistent prediction for F6-1. Consistent tendency in estimation of both bond lengths and bond angles was observed within results

of B3LYP and ωB97XD calculations. However, the obtained bond angles of F6A and F7A at the B3LYP/def2-TZVP level were notably larger than those of all others. Thus, according to the moderate and confident characteristic values, we preferred to suggest ωB97XD/def2-TZVP as a feasible method for futher computations. The optimized structures at the ωB97XD/def2-TZVP level can be seen in Figure 1(iii), which, unless otherwise specified, have been used for all subsequent analyses.

Figure 2 exhibit the IR plots and ^{1}H NMR results, where the IR values of F6A, F7A, F8A, F6E, F7E, and F8E were found to correspond well with the experimentally reported data.[28−32] First, from Figure 2(g−i), it was observed that the absorption vibration peaks of each C−Cl bond were in good symmetry, the wave numbers of which were all within a range of 850−950 cm^{-1}. By comparing the FT-IR diagram of F6-1(g) and F7-1(i), C−Cl peaks showed a slight red shift. Regarding C=C, from F6E(d) to F8E(f), fluorination on C=C obviously moved corresponding peaks to a higher wavenumber field as well. Comparably, in contrast with the C=C absorption vibration peak of F6-1(g), the fluorination and chlorination respectively offered chemicals of F7-1(i) and F6-12(h) a red and blue shift. All these indicated that the introduction of F on C=C contributed to the molecular stability, which was ascribed to the strong electron-absorbing effect of F. Besides, the peak intensity of C=C bonds substituted by H, Cl, and F increased in sequence, indicating the largest dipole distance and polarity of the bond as fluorination occurred.

To verify the above structural correctness, chemical shifts (shielding tensors) and spin−spin coupling constants were further computed using the gauge independent atomic orbital method at the revTPSS/pcSseg-1[58,59] level for all ^{1}H NMR. ^{13}C and ^{19}F NMR images were obtained by using B97-2[60,61] with the same basis set of theory. Excluding that all ^{19}F NMR images were calibrated by shifts of the related nuclei in CFC-11, ^{1}H and ^{13}C NMR images were corrected by TMS (Tetramethylsilane). Chloroform was set to reflect the solvation effect by using the IEFPCM model. For ^{1}H NMR, it can be determined that the results obtained via the ωB97XD functional were quantitively accurate by comparing to previous work by Zhang et al.[23,26,62] Note that actual shielding values for F6A were 2.501 ppm (H6, H7) and 2.283 ppm (H8, H15) before degeneracy, respectively. Clearly, the introduction of the C=C bond gave greater chemical shifts of ^{1}H, and
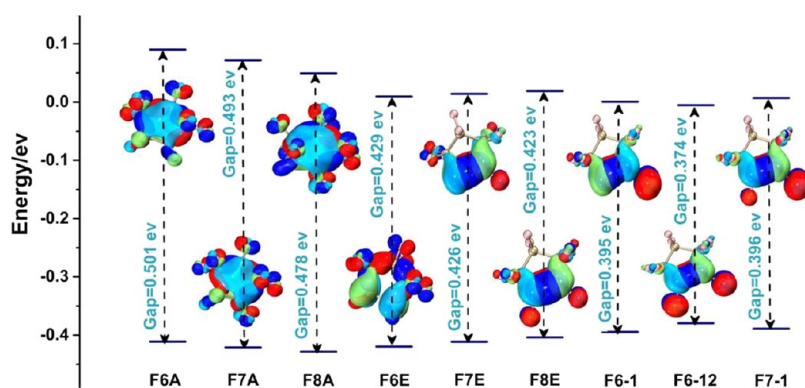
Figure 3. Map of the HOMOs and LUMOs. Red and blue depict the positive and negative phases of HOMOs, respectively, and lime and cyan represent the positive and negative phases of LUMOs, respectively. The isovalue was set as 0.05 for clarity.
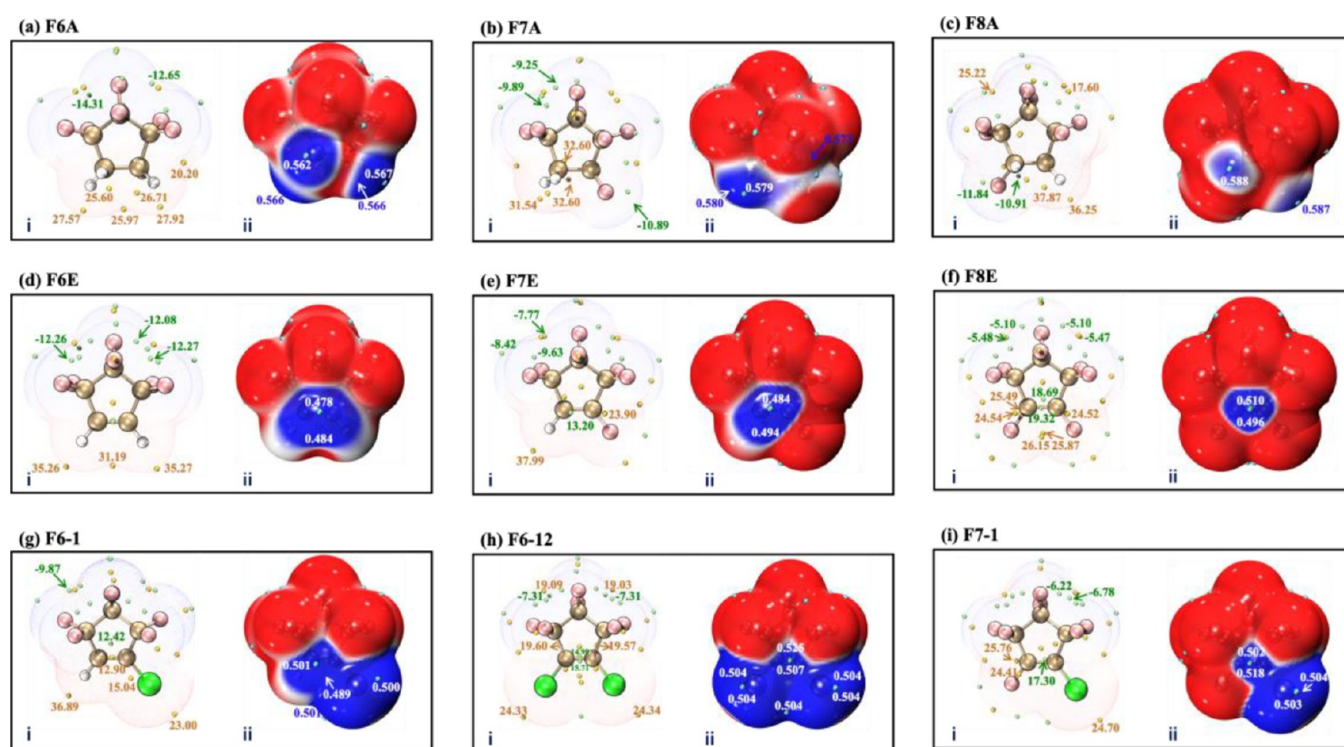

Figure 4. (a−i) Plot of the ESP (i, isovalue = 0.001 a.u.) and ALIE (ii, isovalue = 0.0005 a.u.) analysis. Blue and red correspond to evidently negative and positive ESP or ALIE. The yellow and cyan spheres represent surface local maxima and minima of ESP or ALIE, respectively (unit in kcal/mol for ESP and a.u. for ALIE). The ESP analysis was carried out with the wavefunction information at the ωB97M-V level based on structures obtained at the ωB97XD/def2-TZVP level.

fluorination provided larger chemical shifts for two hydrogen atoms in mirror symmetry. For hydrogens connected to C=C, substitution from fluorine effectively diminished the chemical shift of another hydrogen, where chlorine affected similarly but slightly. This could be ascribed to the greater electron induction capacity of F. Further, qualitatively correct NMR data of ^{13}C and ^{19}F are listed and compared in Table S1, indicating the reliability of the ωB97XD/def2-TZVP method in this work.

3.2. Reactivity and Typical Atmosphere Characters.
3.2.1. Molecular Orbital (MO) Analysis. Fluorination effects will affect the ionization energy and electronic structural properties.[63] As shown in Figure 3, the HOMOs of hydrofluorocyclopentanes resided mainly around all covalent bonds, and their LUMOs comparatively spread over both sides of the cyclic carbon plane. Both two types of MOs were less

localized as the C=C bond was introduced and concentrated around the carbon−carbon bond and further occupied the orbitals of X (X = F and Cl) atoms bonding to the C=C bond. For hydrofluorocyclopentanes including F6A, F7A, and F8A, the introduction of F effectively induced a decrease of the HOMO−LUMO gap, which was ascribed to the strong electron-attracting ability of F, leading to the enlarged negative phase scale of the LUMO and electron-accepting ability. A C=C bond intensively decreased the LUMO energies and transferred the nucleophilic reaction site from uniform distribution to C=C linked atoms and its adjacent carbon bond. For hydrofluorocyclopentenes of F6E, F7E, and F8E, the HOMO−LUMO gap diminished more slightly, indicating the smaller effect of F with the presence of the C=C bond. In contrast, since chlorine was manifested as the preferential electrophilic site, the decreased HOMO−LUMO gaps with
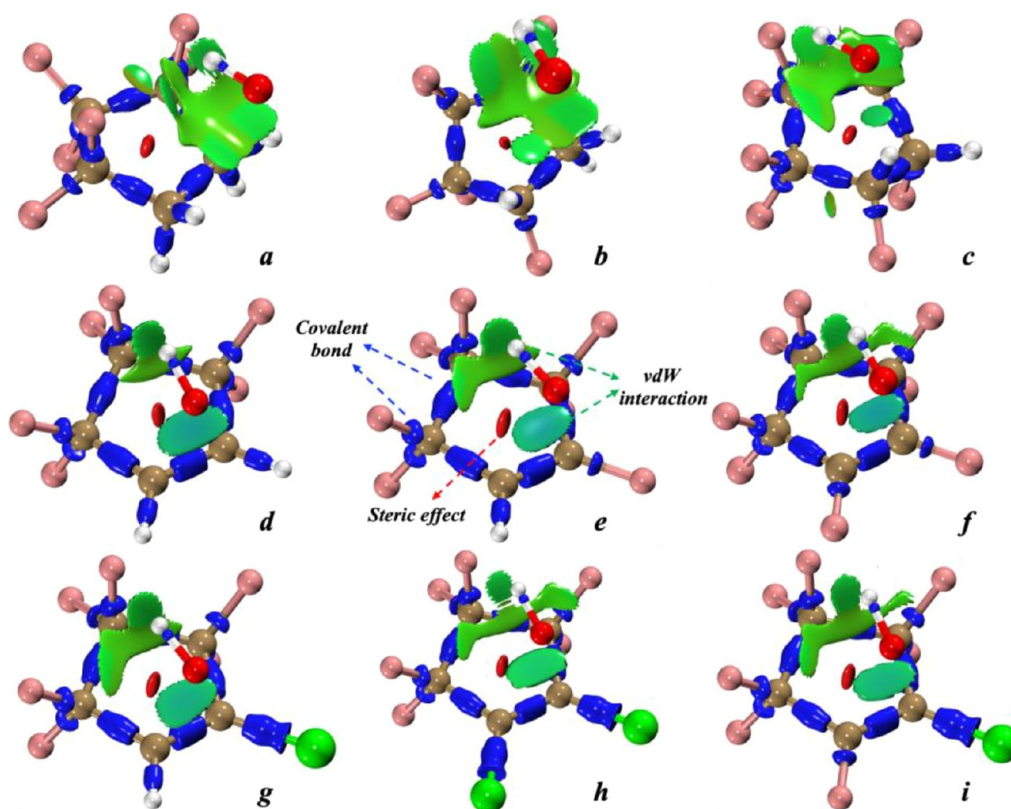
Figure 5. IRI analysis (isovalue =0.9 a.u.) of (a) F6A, (b) F7A, (c) F8A, (d) F6E, (e) F7E, (f) F8E, (g) F6-1, (h) F6-12, and (i) F7-1. Color code: red refers to the steric effect, blue indicates the strong interaction, and green implies area generating weak molecular interactions.

chlorination from hydrogens in F6E, F6-1, and F6-12 were mainly ascribed to the increased HOMO energies, suggesting the stronger ability to release electrons. This indicated that substitutions on c-C$_5$Fs would effectively induce a decrease of the HOMO−LUMO gap and proton affinity and an increase of electron affinity and the molecular reactivity, destabilizing the structures in the sequence of H < F < Cl. Regarding the fluorination from Cl atoms in F6-12, F7-1, and F8E, though their phase maps were similar, substitution of F imparted both lower LOMO and higher HOMO energies, resulting in greater HOMO−LUMO gaps (note: HOMO: the highest occupied molecular orbital; LUMO: the lowest unoccupied molecular orbital).

Besides, based on the theory that the vertical ionization potential (VIP) equals the negative value of the HOMO energy,[64,65] we noticed that substitution of F in alkanes normally implemented the greater ionization energy, while both F and Cl in olefins observably diminished the VIP. Therefore, this demonstrated that fluorinated alkanes are more sophisticated in oxidization, while halogenated alkenes tend to exhibit reducing properties due to the lower oxidation potential.

3.2.2. Molecular Electrostatic Potential Analysis. The atmospheric lifetime of the halogenated compound has been considered to mainly depend on the reaction rate, which belongs to an electrophilic reaction. But how does the substitution of H, Cl, F, and C═C on c-C$_5$Fs distribute the preferentially potentiophilic sites and affect their reactivity? ESP will illustrate this vividly and reveal favorable electrostatic interaction sites.[66−68] As shown in Figure 4, the ESP distribution varied with different substitution atoms around C1 and C2 atoms. For F6A, F6E, and F6-1, maps of ESP on

the electron density isosurface were well divided into two regions with positive and negative ESP values. As c-C$_5$Fs were fluorinated, the minimum negative ESP showed the preferentially potentiophilic sites to attract electrophilic reagents. In contrast with F6A, fluorination of both F7A and F8A induced the more positive ESP on hydrogens and allowed the easier dehydrofluorination to F6E and F7E, consistent with the experiment phenomenon.[24] Both chlorination and C═C bonds contributed to present more but positive ESP minima. This is more conveniently observed from the average local ionization energy (ALIE) analysis.[69] Blue colored area represents the weak electron-binding position that is favorable to electrophilic reactions. In the system of these fluorinated alkanes, hydrogens were more likely to be abstracted according to the minima ALIE values ranging from 0.562 to 0.588 a.u. The smaller ALIE value implied the greater electrophilic reactivity. While a C═C bond commonly imparted smaller ALIE values, which distributed mainly around the double bond, indicating the preferentially potentiophilic points those benefited the hydrodehalogenation on the C(sp2) position instead of the C(sp3) position. This is in good agreement with the previous experimental findings.[26]

3.2.3. van der Waals (vdW) Potential Analysis. Owing to the obviously divided positive and negative ESP regions of above c-C$_5$Fs, the vdW interaction in system is likely to attach great importance. Refs 48−50 theoretically reported the atmospheric degradation of F6E, F7E, and F7A initiated by ·OH radicals, where the reactions of c-HFOs (including F6E and F7E) were considered to proceed through indirect pathways by forming the "precomplexes", namely, the intermediates. However, the fundamental mechanism on such intermediate formation and the leading driving force

were not fully discussed. Therefore, the real-space function analysis of the vdW potential[70] was performed to reveal the vdW interactions between c-C$_5$Fs and the external environment. According to the similar atomic size of neon (Ne) and the halogens that ubiquitously coexisted with c-C$_5$Fs, here we chose Ne as the probe atom. In this work, the required parameters were obtained from the UFF molecular forcefield.[71] Figure S2 exhibits the results that are depicted as an isosurface map, where the local minima points were drawn into red balls for convenient inspection. Note that only the negative isosurface is shown in Figure S2, where dispersion effects exceeded the exchange repulsion. It can be seen that the negative vdW potential isosurface was mainly localized around bonds between C1 and C2. This explained that the strongest vdW attraction could be felt by an atom in the region near the center of the C1−C2 bonds, since it could be attracted by all these c-C$_5$Fs in this area. Although the vdW potential in the peripheral area away from the C1−C2 bond was also negative, its magnitude did not exceed 0.5 kcal/mol. This is because the dispersion attraction attenuates following an inverse sixth power law of the interaction distance r.[72] The vdW potential maps gave us a reason to believe that these cyclic compounds were also able to preferentially adsorb small molecules to or near the C1−C2 bonds owing to obvious dispersion attraction.

Further, possible intermediate complexations of the titled c-C$_5$F chemicals and ·OH radicals were optimized, and the interactions between two fragments were visualized using IRI analysis in the Multiwfn program.[73] In short, the IRI is defined as

$$\text{IRI}(r) = \frac{|\nabla \rho(r)|}{[\rho(r)]^a}$$

where $\rho(r)$ is the electron density, and constant $a = 1.1$. In this method, all IRI isosurfaces between two fragments (i.e., the ·OH radical and the c-C$_5$F) in Figure 5 were basically green, indicating very low electron density in the intermolecular interaction region. This demonstrated that the main driving force for molecular binding was dispersion attraction. Apart from the green pies over C1−C2 bonds, vdW interactions of hydrogen and fluorine were also detected, and the steric effect in the center of the ring was noticed. Therefore, we could safely conclude that in the formation of "precomplexes", there is a lack of strong interactions decisive to their great stability.

The thermodynamic properties of the formation of possible "precomplexes" were also calculated and are later shown in Table S3, where all processes were found to be exothermic and their Gibbs free energies were positive in values, indicating unspontaneous reactions under atmospheric conditions (298.15 K). In order to sufficiently characterize the interaction strength and stability of these intermediate complexes, we carried out a 2000 fs AIMD simulation at 298.15 K temperature at the r2SCAN-3c level. The trajectory frames can be visualized in Videos S1−S6. At approximately 250 and 350 fs, all complexes of these c-C$_5$Fs were observed to transform into corresponding more stabilized geometries, implying their poor stability and that these structures had been destroyed. Hence, a "precomplex" could hardly exist in the atmosphere degrading process.

3.2.4. Atmospheric Properties and the Degradation Mechanism. As a key indicator of environmental performance evaluation for fluorine-containing substances, 100-year global warming potential (GWP$_{100}$) illustrates the relative contribu-

tions of various greenhouse gases to climate change due to the absorption of C−F bonds in the atmospheric window region and their relatively long lifetimes. Normally, GWP can be obtained by the radiative efficiency (RE) and atmospheric lifetime:

$$\text{GWP}_t = \frac{\text{AGWP}(t)}{\text{AGWP}_{\text{CO}_2}(t)} = \frac{A\tau\left(1 - \exp\left(-\frac{t}{\tau}\right)\right)}{\text{AGWP}_{\text{CO}_2(t)}}$$

where A is RE, τ is the atmospheric lifetime, t is the time horizon, and $\text{AGWP}_{\text{CO}_2}(t)$ is the absolute GWP for CO$_2$ within time horizon t.

In this work, atmospheric lifetime was calculated by simulating the reaction rate constant of atmosphere degrading of the titled c-C$_5$F chemicals with OH radicals (the rate-determining step of degradation). The rate constants were calculated based on the transition state theory (TST), which could be expressed as

$$k^{\text{TST}} = \sigma \frac{k_B T}{h}\left(\frac{RT}{P_0}\right)^{\Delta n} e^{-\Delta G^{0,\neq}/(k_B T)}$$

where σ is the degeneracy of the reaction path; k_B is Planck's constant with a value of 1.381×10^{-23} (J/K); h is 6.626×10^{-34} (J·s); R is an ideal gas constant of 8.314 (J/mol/K); and $\Delta n = n - 1$, where n is the number of reactants. $\Delta G^{0,\neq}$ refers to the free energy of activation at the standard state (kJ/mol). The transmission factor of tunneling effect (κ) was taken into consideration according to the Skodje−Truhlar method.[74] Then, atmospheric lifetime was estimated according to a diurnally averaged [OH] (1×10^6 molecule cm^{-3}) with the ·OH rate constant at 298 K.[75]

The possible reaction pathways of c-C$_5$Fs and ·OH radicals were first established and shown in Figure 6. It can be seen that for all hydrogen-containing chemicals, the hydrogen abstraction was considered as an important process rather than any withdrawal of F/Cl atoms.[49] The introduction of the carbon−carbon double bond offered the hydroxyl radical the possibility of addition on the compound, which was recognized as the more dominant reaction process and was fully considered in this work, consistent with ESP and ALIE analyses. For all possible pathways involved herein, the reactivity characters are also exhibited in Table S2, and thermodynamic parameters are tabulated in Table S3. From Table S3, all processes including hydrogen abstraction from c-HFCs and addition in olefins were computed to be spontaneous and exothermic. Besides, in this work, the wavefunction stability should be noted according to the negligible spin contamination with <S^2> = 0.75.

Good correlations between the hereto calculated rate constants and the reported data can be found in Table 1 (more details in Table S2), where results obtained at the ωB97XD/def2-TZVP level could basically provide the great estimation. The short atmosphere lifetime was predicated in the sequence of F6-1 < F7-1 < F7A < F6E < F8E < F7E < F6A < F8A < F6-12. According to the contribution of k_{rate} to GWP, all these chemicals excluding F6-12 were of valid environmental friendliness. However, the difference between k_{rate} obtained experimentally and theoretically of F7A at 298 K was noticed, implying the request of further accurate experiment and better-designed theoretical calculations. This provided evidence and knowledge on the environmental friendliness and considerable degrading rate of these five-membered ring fluorides.
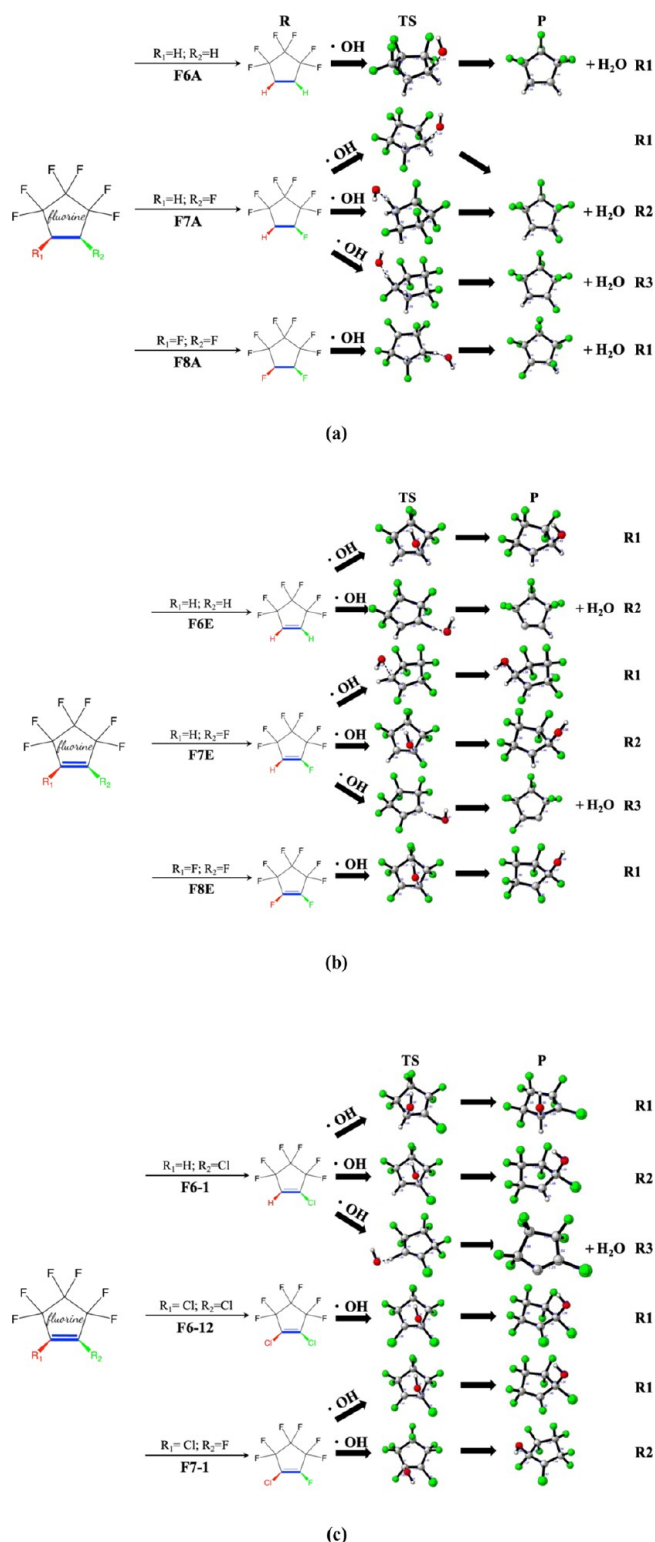
Figure 6. Possible reaction pathways in the degradation of ·OH radicals with (a) c-HFCs, (b) fluorinated five-membered cyclic olefins, and (c) chlorine-containing c-C$_5$Fs. **TS** and **P** refer to corresponding transition states and products, respectively.

3.3. Thermal Stability Characters. 3.3.1. Character of Chemical Bonds. Fluorinated cyclic compounds show peculiar properties including their electronic structure and stability as compared to their chain structures.[76,77] A correct understanding of the chemical bonds' properties will have an

important guiding role in the practically molecular application in the future. In this part, we explored the nature of chemical bonds by means of bond order and natural bond orbital analyses.

3.3.1.1. Bond Order Analysis. To understand the bonding characters beneficial to the thermal stability, Laplacian bond orders (LBOs) of all carbon bonds were computed. In essence, LBO faithfully explains the actual bonding strength.[78] Table 2 clearly demonstrates the single or double bonds in c-C$_5$Fs. It is noteworthy that fluorination induced a decrease of bonding polarity and an increase of the bonding strength. However, chlorination would destabilize the structures and correspondingly gave the C1−C2 bond a larger bonding polarity. Any substitution seemed to have fewer effects on bonds at the *meta*-position. Moreover, we tend to stress the significant role of the C=C bond in stabilizing configurations, and according to the larger LBO values of C2−C3 and C5−C1, the carbon−carbon double bonds were found to contribute not only to the bond itself but also the bonds containing either of its atoms.

3.3.1.2. Natural Bond Orbital (NBO) Analysis. To explore different thermal performances of these c-C$_5$F chemicals, the NBO second-order perturbation analysis[79] was carried out and the stabilization energies (E^2) were computed to evaluate the contribution from the orbital interactions to the stability of these c-C$_5$F compounds. As shown in Table S4, the E^2 values stemmed from the $n_{F(or\ Cl)} \rightarrow \sigma^*_{C-F}$ and $n_{F(or\ Cl)} \rightarrow \pi^*_{C1=C2}$ orbital interactions were large in value. The phase maps of overlapped orbitals are plotted in Figure 7, which respectively induced the largest second-order perturbation energy in each system.

In the NBO analysis, electrons transferred from the lone pair valance NBO orbitals of F or Cl atoms to the antibond (BD*) of C−F bonds or π^* of the C1=C2 bond significantly contributed to their conformational stabilization. According to their unique interaction atoms, three typical orbital interaction types were recognized.

For F8A, the orbital interaction between F12 and C5 (*meta*-carbon)-F13 was found to play the dominant role, where C5−F was the acceptor NBO, while the orbital interaction of F6A, F7A, and F6E that significantly contributed to the structural stabilization belonged to the second type; i.e., the C4 (*para*-carbon)-F acted as the acceptor NBO. The largest $E^{(2)}_{i \rightarrow j^*}$ values greatly contribute to structures' stabilization, which ranged from 22.13 to 22.81 kcal/mol for F6A, F7A, and F8A and 21.71 kcal/mol for F6E, respectively.

The $n_{Cl} \rightarrow \pi^*_{C1=C2}$ orbital interactions substantially enhanced on going from the introduction of the carbon−carbon double bond and Cl for other configurations, and two Cl atoms of F6-12 had the same value of $E^{(2)}_{i \rightarrow j^*}$. As shown in Figure 7, the orbital interactions with the largest $E^{(2)}_{i \rightarrow j^*}$ in F7E, F8E, F6-1, F6-12, and F7-1 belonged to the third type. For compounds substituted with F on the C=C bond, they exhibited much larger $E^{(2)}_{i \rightarrow j^*}$ than others. This suggested the importance of the electrophilicity of C=C and the nucleophilicity of the X atom (X = F or Cl) for the orbital interactions.

3.3.2. Thermal Stability Simulation. As explained above, the c-C$_5$Fs have been utilized in electronic cleaning, etching, heat pump fluid, etc. In these practical applications, great performance is inseparable from the thermal stability in the system, especially when it is directly related to storage capacity and durability. Consequently, we further conducted the AIMD computation to reveal the relevant thermal behavior in the

Table 1. Rate and Atmosphere Properties of the Titled c-C$_5$Fs, Where Only the k_{rate} Based on the Most Possible Degrading Pathway Was Tabulated

| | k_{rate} (cm^3 molecule^{-1} s^{-1}, ×10^{-13}) | | | atmosphere lifetime[d] | GWP$_{100}$ |
c-C$_5$Fs	ωB97XD[a]	M06-2X[b]	ref	τ/d	ref
F6A	0.650	0.256	0.294 ± 0.005[28]	178.09	107[28]
F7A	1.863	1.234	0.172 ± 0.005[29]	62.13	211[29]
F8A	0.475	0.812	0.143 ± 0.003[29]	243.46	241[29]
F6E	1.815	2.737	1.08 ± 0.04[30]	63.77	15[30]
F7E	0.923	1.454	0.520 ± 0.009[31]	125.41	42[31]
F8E	2.066 (0.978)[c]	2.657	1.01 ± 0.16[32]	118.34	28[32]
F6-1	6.688	5.476		17.31	
F6-12	0.110	0.132		1051.23	
F7-1	1.989	2.348		58.19	

[a]Results obtained at the ωB97M-V/def2-QZVP//ωB97XD/def2-TZVP level, which means that the geometries were optimized at the ωB97XD/def2-TZVP level and energies were calculated at the ωB97M-V/def2-QZVP level. [b]Results obtained at the ωB97M-V/def2-QZVP//M06-2X/def2-TZVP level. [c]Values in parentheses were obtained at the ωB97XD/def2-TZVP level. [d]Atmosphere lifetime was obtained at the ωB97M-V/def2-QZVP//ωB97XD/def2-TZVP level.

Table 2. LBO of Carbon Bonds in the Studied Five-Membered Ring Fluorides

| | bonds | | | | |
c-C$_5$F	C1−C2	C2−C3	C3−C4	C4−C5	C5−C1
F6A	0.912932	1.081611	1.064938	1.008900	1.020276
F7A	0.988410	1.081313	1.057076	1.007962	1.015297
F8A	1.055047	1.034412	0.942588	1.007380	1.072934
F6E	1.909154	1.173698	1.003788	1.003788	1.173699
F7E	1.947056	1.177160	0.996675	0.993515	1.165666
F8E	1.962669	1.181574	0.988178	0.988366	1.181136
F6-1	1.863361	1.094170	0.992038	1.008904	1.160472
F6-12	1.790019	1.081784	0.996785	0.996787	1.081780
F7-1	1.882216	1.168402	0.998001	0.981951	1.094665
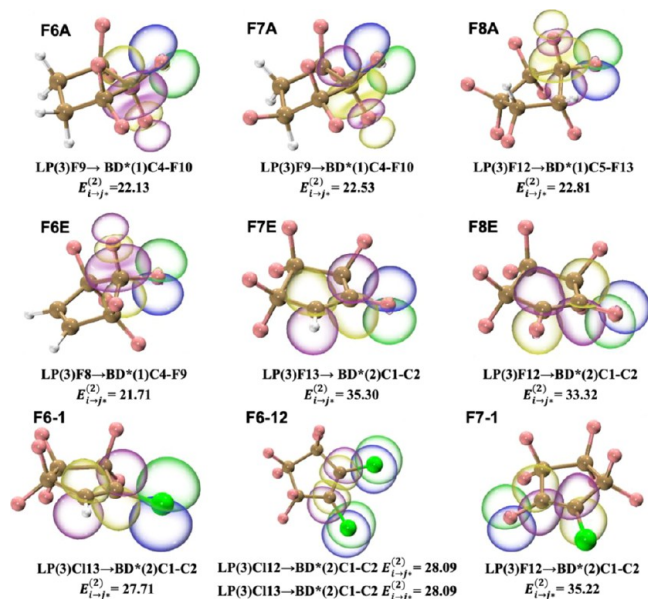
Figure 7. Plots of NBO analysis. Green and blue depict the positive and negative phases of donor atomic orbitals, respectively, and yellow and purple represent the positive and negative phases of acceptor atomic orbitals, respectively. The isovalue was set as 0.05 for clarity.

realistic environment. Then, 2000 fs simulation at a temperature of 600.00 K was carried out using the r2SCAN-3c method in the ORCA program and is shown in Figure 8(i).

Since the stability of the carbon ring structure always gained more interest, we omitted the atomic motion of H, F, and Cl for clarity. The **GIFs** documenting the MD trajectory can be seen in Videos S7−S15. It can be found that at 600 K, structural deformation of these cyclic fluorides occurred but was inconspicuous within the limited simulation time, demonstrating their relative stability. The flexible characteristics of the five-membered ring carbonic skeleton were further recommended, where the thermal motion mainly took place in out-plane with less in-plane deformation.

Moreover, in Figure 8(i), a greater amplitude variation of C1 and C2 atoms in c-HFCs was observed, implying a distortion tendency to other isomerization structures. The C=C bonds efficiently enhanced the molecular thermostability, where fluorination also showed significant roles. However, according to the nonoverlapped red and blue balls in F6-1, F6-12, and F7-1, substitution from chlorine was not conducive enough to more stabilized configurations, which exhibited out-of-plane deformed structures instead. Therefore, the thermostability of F8E could be confirmed, followed by F7E and F6E, consistent with their experimentally observed pyrolysis temperatures.

To precisely gain the information of bonds' stability, LBO was computed to understand the bond characteristics along the trajectory, and the tendency is plotted in Figure 8(ii−iv). Since the C1−C2 bond was directly affected by substitution effects, the bond order of all C1−C2 bonds was analyzed. It can be seen that the LBO of C1−C2 in hydrofluorocyclopentanes vibrated randomly, and the strength of C1−C2 bonds exhibited an overall trend of F8A > F7A > F6A though some LBO overlapped. For olefins, the vibration of LBO varied with the obviously narrower range. Another notable characteristic was that LBO changes of F6E and F8E gradually converge to the original LBO over time, indicating that their in-plane (stretch deformation) thermal stability should be emphasized due to their "self-recovery" ability. Both LBOs of F6-12 and F7-1 were forced into more regular changes and reached the greatest deformation at 500−750 fs (<1.2) and 1750 fs (<0.9), respectively (corresponding to light red and blue in Figure 8(i), respectively). Notably, we want to stress the great thermal performance of F6-1 within simulating timescale, the LBO of which changed with a maximum deviation (<0.6) at around 1750 fs, illustrating its important in-plane stability. Besides, for all chlorine-containing molecules, the max LBO deviation
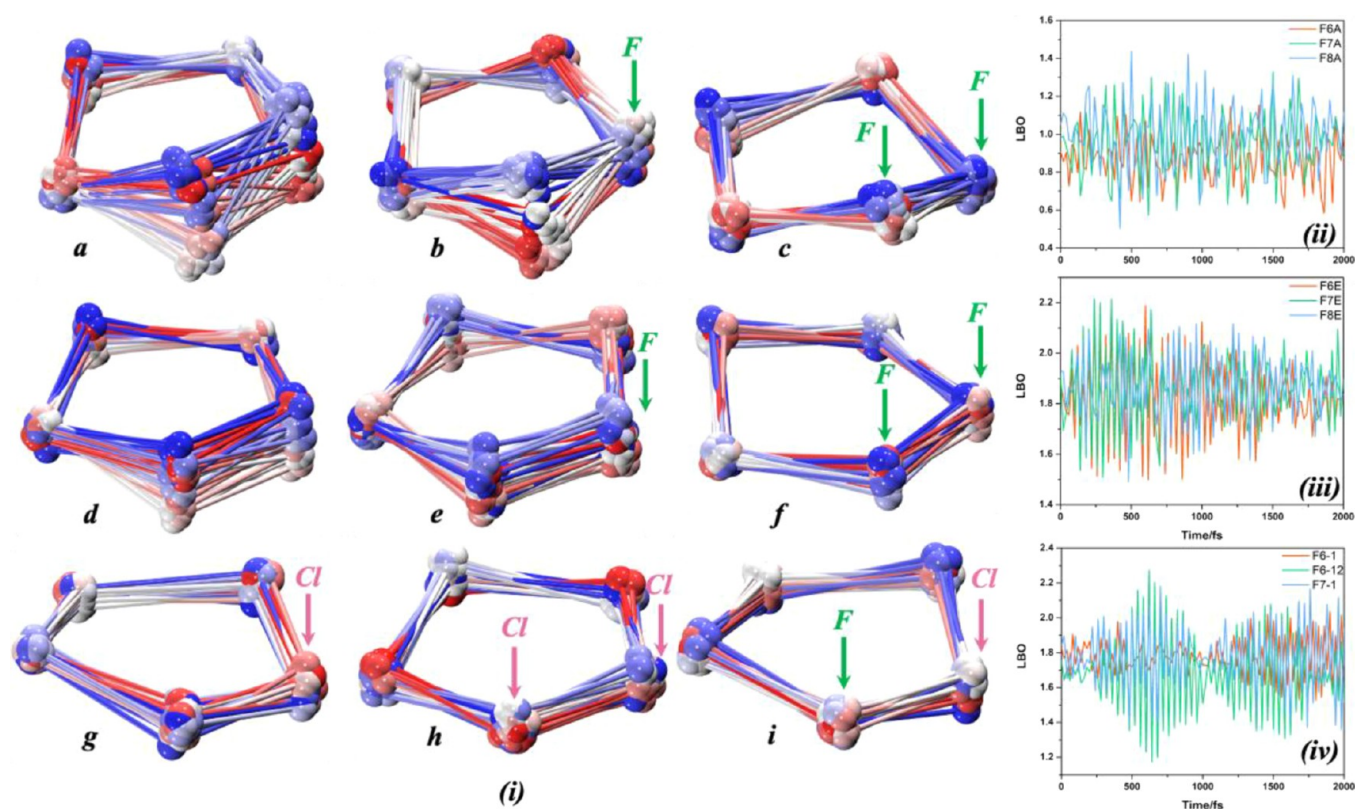
Figure 8. (i) 2000 fs trajectory of AIMD simulation of (a) F6A, (b) F7A, (c) F8A, (d) F6E, (e) F7E, (f) F8E, (g) F6-1, (h) F6-12, and (i) F7-1 at 600.00 K. The structures are drawn every 50 fs, and the color represents timestep and varies as red−white−blue. (ii)−(iv) Tendency plots of LBO of c-C₅Fs within 2000 fs, which are depicted every 20 fs time step.

decreased in the presence of Cl > F > H, which is consistent with the ESP analysis.

Further, plots of planarity tendency along the AIMD simulation trajectory were analyzed through the Multiwfn program and are shown in Figure 9. As can be seen, the planarity of these ring fluorides almost fluctuated periodically. The planarity of F7A and F8A varied every 500 fs per cycle, while that of F6A changed more irregularly. The planarity of fluorine-containing olefins except F6-1 varied with a longer period, both MPP (molecular planarity parameter) and SDP (span of deviation from plane) of which exhibited a larger deviation, confirming that the out-plane deformation of these cyclic olefins was easier. The strong out-plane stability of F6-1 was then concluded according to its smallest MPP and SDP.

In summary, the thermostability of F8E, F7E, F6E, and F6-1 should be significantly stressed, where that of F8E, F6E, and F6-1 was attributive to their in-plane and out-plane stability, respectively. This provided theoretical guidance and reliable basis for future application of these c-C₅Fs in a more rigorous working environment.

3.3.3. Aromaticity Analysis. Aromaticity plays a significant role in the stability of circular molecules. Notably, the isolated structures of these c-C₅Fs are in fact nonplanar at equilibrium, but for substitution effect from C=C bonds, they could be easily restricted to almost the plane, establishing the basic premise for an aromaticity.

3.3.3.1. Iso-Chemical Shielding Surface (ICSS) and Nucleus-Independent Chemical Shifts (NICS). The ICSS[80] is a real-space function closely related to the famous NICS,[81] which can effectively evaluate the aromaticity of ring molecules. The NICS studies chemical shielding at specific

points against the external magnetic field, while the ICSS investigates this in a three-dimensional spatial scale. We first investigated the negative value of the magnetic shield at 1 Å above the ring center point (NICS(1)_ZZ) in Figure 10. The center of a ring was defined according to the mass center of the carbonic ring. As shown in Figure 10, the only negative value of total NICS(1)_ZZ in F6E was observed, which was essentially ascribed to the shield effect against the external magnetic field generated by the ring-current-induced magnetic field over the ring.

To evaluate aromaticity more reliably, the ICSS maps shown in Figure 11(a), where the magnetic shielding area was fairly large and smooth. The green isosurface represents the area with a magnetic shield value of 0.025, and the cyan isosurface represents the area with a deshielding value of 0.025. It can be seen that molecules were surrounded by the green isosurface, indicating the magnetic shielding effect of the local circulation of electrons from sigma bonds. The shielding area is normally accompanied by the deshielding area; thus, a blue deshielding isosurface was always noticed in system. However, only F6E exhibited the continuous ring current as compared to others. The results of induced ring current illustrated that F6E was indeed aromatic and could induce a general ring current and shield the magnetic field in the inner region obviously. To illustrate this more clearly, the isosurface of the ZZ component of the ICSS (ICSS_ZZ) of F6E is presented in Figure 11(b). The cross-section along the YZ plane of this isosurface was chosen for clarity. We noticed that there were significant shielding regions protruding in the direction perpendicular to the ring plane of C1−C2−C3−C4−C5 and a closed deshielding circular isosurface surrounded it. Also, 2.50 ppm was identified
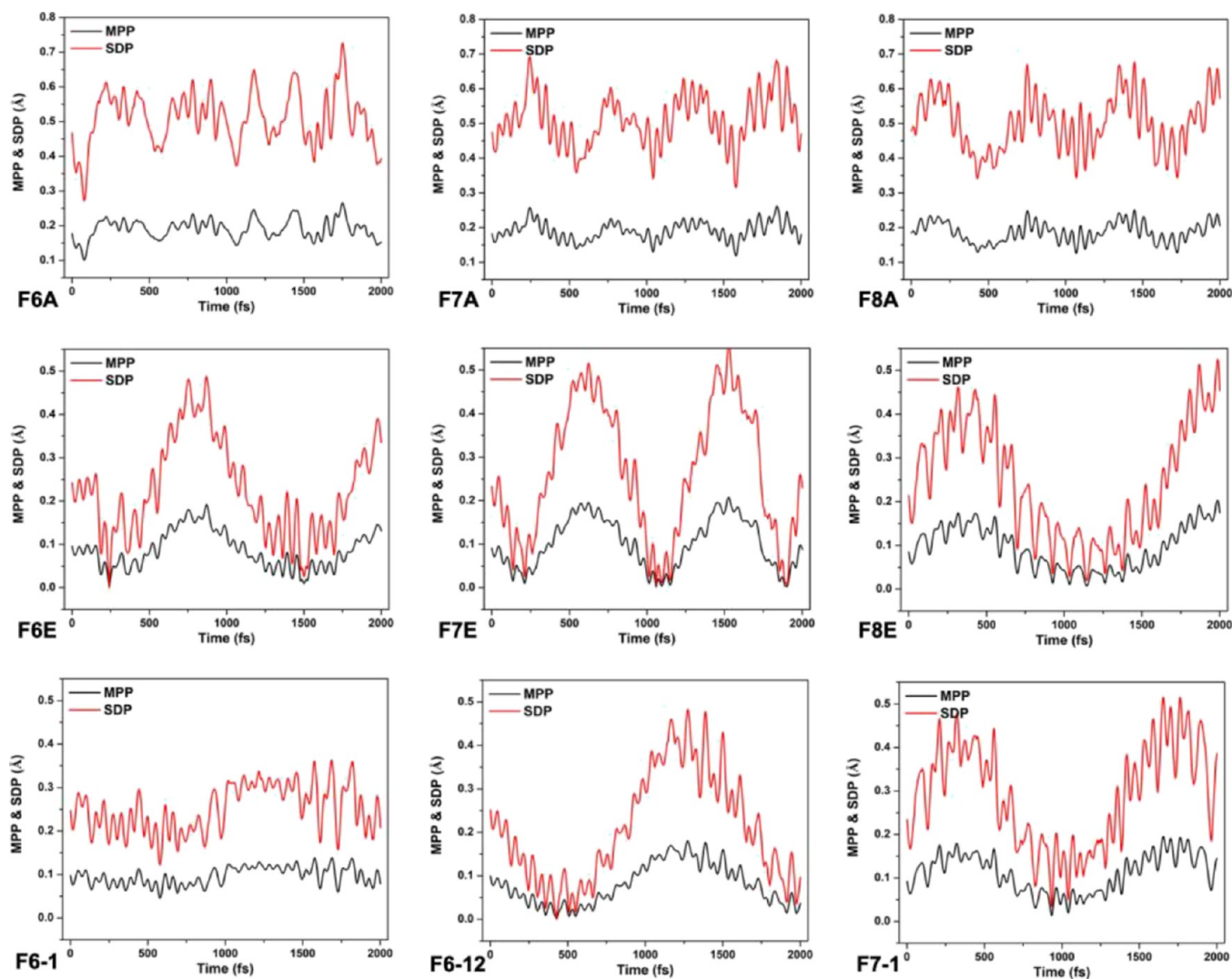
Figure 9. Plot of planarity tendency along the AIMD simulation trajectory (at 600.00 K).
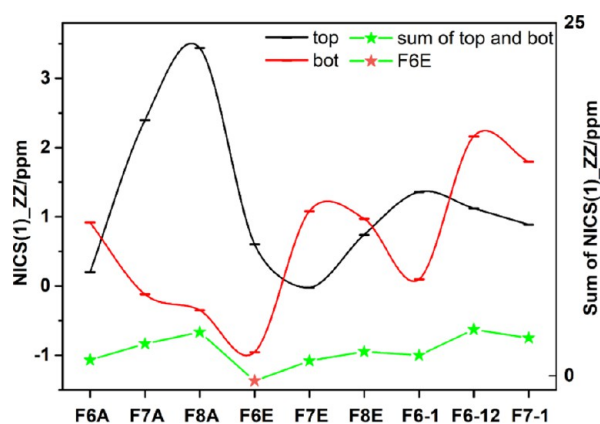

Figure 10. NICS(1)_ZZ plots of the studied c-C_5Fs, where top and bot refer to the NICS(1)_ZZ values obtained at both the top and bottom sides of the ring plane, respectively.

as the critical point to recognize a continuous isosurface, implying the slight aromaticity.

3.3.3.2. Anisotropy of Current-Induced Density. Ring current is, according to a widely accepted concept, a defining characteristic of aromatic systems.[81,82] ACID analysis was

further performed to reveal the strength of isotropy induced by electrons at the corresponding position to the external magnetic field. From Figure 11(c), two kinds of ring current contributed by out-ring and in-ring electrons were observed. The current induced by out-ring electrons followed the left-hand rule, confirming the relative aromaticity of F6E, while the in-ring electrons induced the paratropic ring current, implying a slight antiaromaticity.

3.3.3.3. Electron Localization Function (ELF).[83] Another real-space function we adopted to reveal the electronic localization character was the ELF. For F6E, since delocalization of π electrons occurred only at the C=C bond, ELF considering orbitals beyond π (i.e., the ELF-σ) is shown in Figure 11(d). The bifurcation point of ELF-σ corresponds to where the entire ELF-σ isosurface starts to split into two as the isovalue increases. At the bifurcation point, the higher the ELF-σ value, the easier the σ electron delocalization between the two ELF domains it connects. As can be seen, the smallest bifurcation point (0.63) was located around the C=C bond, indicating moderate sigma delocalization over carbon rings. The σ electrons making up the C=C bond were thus decisive to induced ring current in this region. Hence, it can be concluded that F6E, clamped by electronically innocent hydrogens rather than F or Cl, was able to show exactly slight
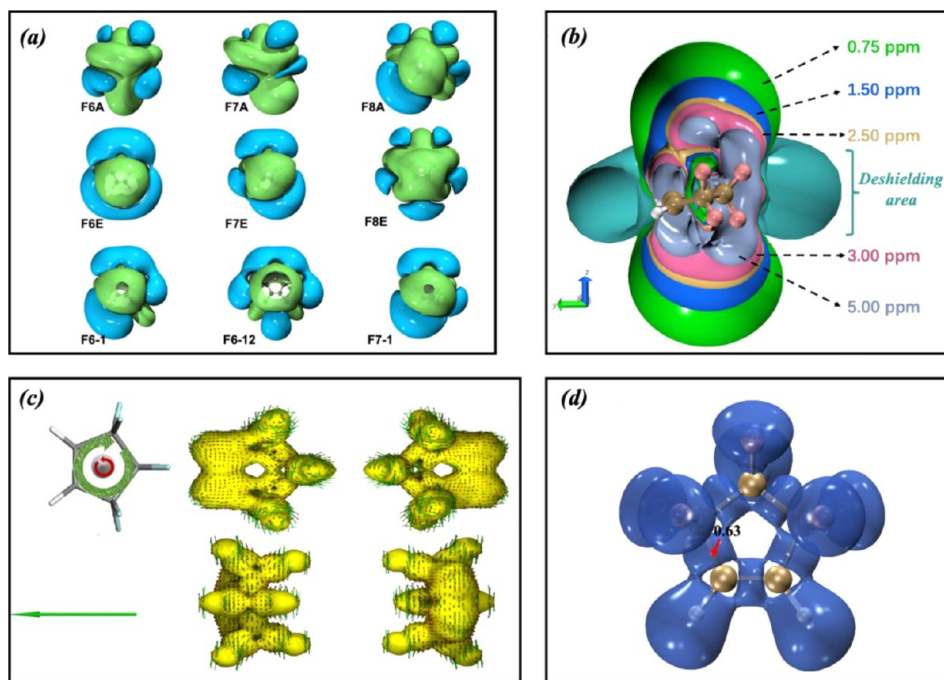
Figure 11. (a) ICSS maps of c-C_5Fs (isovalue = 0.025); (b) ICSS$_{ZZ}$ map of F6E; (c) isosurface map of ACID of F6E, isovalue = 0.025. The green arrows represent the direction and magnitude of the ring current at various positions. Arrows with length smaller than 1 are omitted for clarity. (d) Isosurface map of ELF-sigma of F6E (isovalue = 0.63).

aromaticity. Compared with chain hydrocarbon compounds, this undoubtedly plays an important role in its greater thermal stability.

4. CONCLUSIONS

As significant potential CFC substitutes, the application of c-C_5Fs has been explored in fields including heat transfer fluids, detergents, solvents, electrolyte, etching gas, extinguishing agents, and so on.

In this work, based on reliable computational methods, the reactivity was first comprehensively investigated. Substitutions were found to notably diminish the HOMO−LUMO gap and enhance the molecular reactivity in the sequence of H > F > Cl, while the C=C bond redistributed both electrophilic and nucleophilic sites effectively. In combination with the ESP and ALIE analyses, the preferential electrophilic site of C=C and hydrogens of c-HFCs were found conductive to their atmosphere degradation initiated by ·OH radicals. This guaranteed c-C_5Fs as feasible CFC substitutes with great environmental properties. Further, combined vdW, AIMD, and thermodynamic studies demonstrated that the formation of stable intermediates in these atmospheric degrading processes of c-C_5Fs was hardly possible, which was more likely to be a one-step reaction mechanism instead, correcting the previous conclusions.

Then, the AIMD simulation (600 K) revealed the strong thermostability of such c-C_5F chemicals due to their flexible carbon skeletons in compounds, where the out-plane stability of F6-1 and in-plane stability of F6E and F8E were peculiarly emphasized. Further, the aromaticity of F6E stemming from π-electron delocalization over the C=C and strong effect of σ-electrons was conductive to its stability.

This work thus throws light on application of these c-C_5F chemicals and molecular design of fluorine-containing organics in the future.

■ ASSOCIATED CONTENT

ⓈI Supporting Information

The Supporting Information is available free of charge at https://pubs.acs.org/doi/10.1021/acsomega.2c02461.

> Details of planarity of c-C_5Fs, NMR data of c-C_5Fs, van der Waals (vdW) potential analysis, atmospheric degrading reaction properties, and NBO data of the titled c-C_5Fs; (**Figure S1**) planarity of the studied c-C_5Fs; (**Figure S2**) vdW potential of the titled c-C_5Fs (isovalue = 0.55); minima highlighted with red spheres (in kcal/mol); (**Table S1**) NMR chemical shifts of all titled five-membered ring fluorides; diff is the percentage of the unsigned difference of both calculated and experimental data to experimental results; (**Table S2**) reactivity characters of the studied five-membered ring fluorides with OH radicals; (**Table S3**) Gibbs free energy (G) and the enthalpy (H) calculated at the ωB97XD/def2-TZVP level; G_1 and H_1 refer to the thermodynamic parameters of formation of "precomplexes"; G_2 and H_2 refer to the thermodynamic parameters of reactions of the studied five-membered ring fluorides with OH radicals; and (**Table S4**) donor and acceptor NBOs and the corresponding stabilization energies (E^2) (PDF)

Trajectory Videos 1−6: **GIFs** documenting the MD trajectory frames of possible "precomplexes" (GIF) (GIF) (GIF) (GIF) (GIF) (GIF)

Video 7: **GIFs** documenting the MD trajectory for F6A (GIF)

Video 8: **GIFs** documenting the MD trajectory for F7A (GIF)

Video 9: **GIFs** documenting the MD trajectory for F8A (GIF)

Video 10: **GIFs** documenting the MD trajectory for F6E (GIF)

Video 11: **GIFs** documenting the MD trajectory for F7E (GIF)

Video 12:**GIFs** documenting the MD trajectory for F8E (GIF)

Video 13:**GIFs** documenting the MD trajectory for F6-1 (GIF)

Video 14: **GIFs** documenting the MD trajectory for F6-12 (GIF)

Video 15: **GIFs** documenting the MD trajectory for F7-1 (GIF)

■ AUTHOR INFORMATION

Corresponding Authors

Xiaoxun Ma − *School of Chemical Engineering, Northwest University, Xi'an, Shaanxi 710069, China;* ⊙ orcid.org/0000-0002-1603-5641; Email: maxym@nwu.edu.cn

Hengdao Quan − *School of Chemistry and Chemical Engineering, Beijing Institute of Technology, Beijing 100081, China;* Present Address: National Institute of Advanced Industrial Science and Technology−Interdisciplinary Research Center for Catalytic Chemistry, 1-1-1 Higashi, Tsukuba, Ibaraki, 305-8565, Japan (H.Z.); ⊙ orcid.org/0000-0003-3130-3162; Email: quanhengdao@bit.edu.cn

Authors

Tongyun Zhang − *School of Chemical Engineering, Northwest University, Xi'an, Shaanxi 710069, China*

Chengping Zhang − *School of Chemistry and Chemical Engineering, Beijing Institute of Technology, Beijing 100081, China*

Complete contact information is available at:
https://pubs.acs.org/10.1021/acsomega.2c02461

Author Contributions

T.Z.: investigation, writing original draft, and visualization. C.Z.: literature investigation and data curation. X.M.: conceptualization, writing, editing, and supervision. H.Q.: project administration.

Notes

The authors declare no competing financial interest.

■ REFERENCES

(1) Zhang, C. P.; Qing, F. Y.; Jia, X. Q.; Quan, H. D. Synthesis and application of five-membered ring fluoride. *CIESC J.* **2020**, *71*, 3963−3978.

(2) Qing, F. Y. *Investigation on synthesis and cleaning performance of hydrofluorocyclopentane*; Beijing Institute of Technology: Beijing, 2019.

(3) Yamada, C.; Tanaka, K. Hard coat agent composition and hard coat film using the same. CN 103102793A, May 15, 2013.

(4) DeGroot, R. J.; Shellef, D. Azeotrope compositions containing a fluorocyclopentane. US7067468B2, June 27, 2006.

(5) Kang, S. Y.; Sawada, I.; Kondo, Y.; Ventzek, P. L. G. Plasma chemistry of octafluorocyclopentene/argon/oxygen mixtures. *Jpn. J. Appl. Phys.* **2008**, *47*, 6843−6848.

(6) Otsuki, N. Environmentally friendly fluorinated cleaning agent ZEORORA ® H. *Industrial Cleaning* **2015**, *15*, 29−35.

(7) Zhou, X.; Lu, D.; Chao, M.; Chen, W. Experimental and theoretical studies on the thermal decomposition of 1,1,2,2,3,3,4-heptafluorocyclopentane. *J. Fluorine Chem.* **2014**, *164*, 70−77.

(8) Usami, Y.; Inagaki, Y. Preparation of optical information recording disc and dye solution. 1213419C, 3 August, 2005.

(9) Tanuma, T. Process for producing membrane/electrode assembly for polymer electrolyte fuel cell. 101946350A, 12 January, 2011.

(10) Zhang, R. W.; Shang, W. Y. A low temperature lithium ion battery. CN 113451556, 28 September, 2021.

(11) Sievert, A. C.; Nappo, M. J.; Minor, B. H.; et al. Compositions Comprising Fluoroolefins and Uses Thereof. CN 2626183 A1, 10 May, 2007.

(12) Clodic, D.; Riachi, Y.; Koban, M. Method for Exchanging Heat in a Vapor Compression Heat Transfer System and a Vapor Compression Heat Transfer System Comprising an Intermediate Heat Exchanger with a Dual-Row Evaporator or Condenser. CN 2682312 C, 22 November, 2016.

(13) Wajima, K.; Matsukura, N.; Ueda, K.; et al. Heat source machine and operating method therefor. JP2017141372, 17 August, 2017.

(14) Toshio, H.; Kenji, I.; Makoto, S.; Masaru, H. Dissociations of C_5F_8 and C_5HF_7 in Etching Plasma. *Jpn. J. Appl. Phys.* **2013**, *52*, No. 05EB02.

(15) Sugimoto, T.; Suzuki, T.; Konagawa, J. Method for producing hydrogen-containing fluoroolefin compound. U.S. Patent 8318991 B2, 27 November, 2012.

(16) Ji, B.; Badowski, P. R.; Motika, S. A.; et al. Evaluating the performance of c-C_4F_8, c-C_5F_8, and C_4F_6 for critical dimension dielectric etching (EB/OL). https: //www. Air products. com/e-newsletters/solutions update/pdf/C_4F_6 Application Notes.Pdf.

(17) Motomura, H.; Imai, S.; Tachibana, K. Difference between C_4F_8 and C_5F_8 plasmas in surface reaction processes for selective etching of SiO_2 over Si_3N_4. *Thin Solid Films* **2000**, *374*, 243−248.

(18) Takahashi, K.; Itoh, A.; Nakamura, T.; Tachibana, K. Radical kinetics for polymer film deposition in fluorocarbon (C_4F_8, C_3F_6 and C_5F_8) plasmas. *Thin Solid Films* **2000**, *374*, 303−310.

(19) Quan, H. D.; Zhang, C. P.; Guo, Q. Fluorine-containing heat transfer fluid, preparation method and application thereof. CN 202010692380.5, 17 July, 2020.

(20) Quan, H. D.; Guo, Q.; Zhang, C. P. Heat transfer device and method. CN 202010692353.8, 17 July, 2020.

(21) Quan, H. D.; Feng, S. W.; Jia, X. Q.; Qing, F. Y.; Zhang, C. P. Environmentally friendly alternative: Synthesis and application of 1-chloro-3,3,3-trifluoropropene. *Fine Chemicals* **2022**, *39*, 677−688.

(22) Quan, H. D.; Tamura, M.; Gao, R. X.; Sekiya, A. Preparation and application of porous calcium fluoride-a novel fluorinating reagent and support of catalyst. *J. Fluorine Chem.* **2002**, *116*, 65−69.

(23) Qing, F. Y.; Zhang, C. P.; Quan, H. D. Synthesis of hydrofluorocyclopentanes by vapor-phase catalytic hydrodehalogenation. *J. Fluorine Chem.* **2018**, *213*, 61−67.

(24) Zhang, W. N.; Zhang, C. P.; Guo, Q.; Lu, F. N.; Quan, H. D. Synthesis of hydrofluorocycloolefins through dehydrofluorination of hydrofluorocycloalkanes in amide solvents. *J. Fluorine Chem.* **2019**, *226*, 109342.

(25) Zhang, C. P.; Qing, F. Y.; Quan, H. D.; Sekiya, A. Synthesis of 1,1,2,2,3,3,4-heptafluorocyclopentane as a new generation of green solvent. *J. Fluorine Chem.* **2016**, *181*, 11−16.

(26) Yang, G.; Zhang, C. P.; Yang, H.; Quan, H. D. Synthesis of 1H-polychlorofluorocycloolefins. *J. Fluorine Chem.* **2018**, *216*, 96−101.

(27) Zhang, C. P.; Qing, F. Y.; Quan, H. D.; Sekiya, A. Investigation on Cl-F exchange mechanism occurring at $C(sp^2)$ and $C(sp^3)$ orbitals of halogenated cyclopentene. *J. Fluorine Chem.* **2016**, *191*, 84−89.

(28) Guo, Q.; Zhang, N.; Uchimaru, T.; Chen, L.; Quan, H. D.; Mizukado, J. J. Atmospheric chemistry for gas-phase reactions of cyc-$CF_2CF_2CF_2CHXCHX$- (X = H or F) with OH radicals in the temperature range of 253-328 K. *Atmos. Environ.* **2019**, *215*, No. 116895.

(29) Zhang, N.; Chen, L.; Uchimaru, T.; Qing, F. Y.; Mizukado, J. J.; Quan, H. D.; Suda, H. Kinetics of gas-phase reactions of cyc-$CF_2CF_2CF_2CHFCH_2$ and trans-cyc-$CF_2CF_2CF_2CHFCHF$ with OH radicals between 253 and 328K. *Chem. Phys. Lett.* **2015**, *639*, 199−204.

(30) Guo, Q.; Zhang, N.; Uchimaru, T.; Chen, L.; Quan, H. D.; Mizukado, J. J. Atmospheric chemistry of cyc-CF$_2$CF$_2$CF$_2$CH=CH-: Kinetics, products, and mechanism of gas-phase reaction with OH radicals, and atmospheric implications. *Atmos. Environ.* **2018**, *179*, 69−76.

(31) Liu, D. P.; Qin, S.; Li, W.; Zhang, D.; Guo, Z. K. Atmospheric chemistry of 1H-heptafluorocyclopentene (cyc-CF$_2$CF$_2$CF$_2$CF=CH-): rate constant, products, and mechanism of gas-phase reactions with OH radicals, IR absorption spectrum, photochemical ozone creation potential, and global warming potential. *J. Phys. Chem. A* **2016**, *120*, 9557−9563.

(32) Wallington, T. J.; Hurley, M. D. Atmospheric chemistry of hexafluorocyclobutene, octafluorocyclopentene, and hexafluoro-1, 3-butadiene. *Chem. Phys. Lett.* **2011**, *507*, 19−23.

(33) Tan, S. S.; Reed, M. L.; Han, H. T.; Boudreau, R. Mechanisms of etch hillock formation. *J. Microelectromech. Syst.* **1996**, *5*, 66−72.

(34) Wu, Z.; Ji, Y.; Li, H.; Bi, F.; Ren, Y. Q.; Gao, R.; Liu, C.; Li, L.; Zhang, H.; Zhang, X.; Wang, X. Study on the pyrolysis characteristics of a series of fluorinated cyclopentenes and implication of their environmental influence. *Chem. Phys. Lett.* **2021**, *764*, No. 138213.

(35) Frisch, M. J.; Trucks, G. W.; Schlegel, H. B.; Scuseria, G. E.; Robb, M. A.; Cheeseman, J. R.; et al. *Gaussian 16, revision C.01*; Gaussian, Inc.: Wallingford, CT, 2019.

(36) Chai, J. D.; Head-Gordon, M. Long-range corrected hybrid density functionals with damped atom-atom dispersion corrections. *Phys. Chem. Chem. Phys.* **2008**, *10*, 6615−6620.

(37) Weigend, F.; Ahlrichs, R. Balanced basis sets of split valence, triple zeta valence and quadruple zeta valence quality for H to Rn: Design and assessment of accuracy. *Phys. Chem. Chem. Phys.* **2005**, *7*, 3297−3305.

(38) Ishida, K.; Morokuma, K.; Komornicki, A. The intrinsic reaction coordinate. An ab initio calculation for HNC→HCN and H$^-$+CH$_4$→ CH$_4$+ H$^-$. *J. Chem. Phys.* **1977**, *66*, 2153−2156.

(39) Mardirossian, N.; Head-Gordon, M. ωB97M-V: A combinatorially optimized, range separated hybrid, meta-GGA density functional with VV10 nonlocal correlation. *J. Chem. Phys.* **2016**, *144*, 214110.

(40) Neese, F. Software update: the ORCA program system, version 4.0. *WIREs Comput. Mol. Sci.* **2018**, *8*, No. e1327.

(41) Lu, T.; Chen, Q. X. Shermo: A general code for calculating molecular thermodynamic properties. *Comput. Theor. Chem.* **2021**, *1200*, No. 113249.

(42) Lucas Bao, J. W.; Zheng, J.; Alecu, I. M.; Lynch, B. J.; Zhao, Y.; Truhlar, D. G. Database of Frequency Scale Factors for Electronic Model Chemistries (Version 3 Beta 2). https://comp.chem.umn.edu/freqscale/version3b2.htm. (Accessed on Dec 25, 2021).

(43) Grimme, S.; Hansen, A.; Ehlert, S.; Mewes, J. M. r2SCAN-3c: An efficient "Swiss army knife" composite electronic-structure method. *J. Chem. Phys.* **2021**, *154*, No. 064103.

(44) Geuenich, D.; Hess, K. K.; Köhler, F.; Herges, R. Anisotropy of the induced current density (AICD), a general method to quantify and visualize electronic delocalization. *Chem. Rev.* **2005**, *105*, 3758−3772.

(45) Povray. Persistence of vision raytracer, POV-Ray 3.7: http://www.povray.org/ (accessed on Dec 25, 2021).

(46) Lu, T.; Chen, F. Multiwfn: A multifunctional wavefunction analyzer. *J. Comput. Chem.* **2012**, *33*, 580−592.

(47) Humphrey, W.; Dalke, A.; Schulten, K. VMD: Visual molecular dynamics. *J. Mol. Graphics* **1996**, *14*, 33−38.

(48) Bhuvaneswaria, R.; Senthilkumar, K. First Principle Studies on the Atmospheric Oxidation of HFC-C1436 Initiated by OH radical. *New J. Chem.* **2020**, *44*, 2070−2082.

(49) Parineeta, G.; Subrata, P.; Bhupesh, K. M.; Gour, N. K.; Deka, R. C. Tropospheric Oxidation of 1H-Heptafluorocyclopentene (cyc-CF$_2$CF$_2$CF$_2$CF=CH-) with OH Radicals: Reaction Mechanism, Kinetics, and Global Warming Potentials. *ACS Earth Space Chem.* **2021**, *5*, 1792−1800.

(50) Chen, W.; He, J.; Jiang, Y.; Zhang, H.; Zhou, X. Experimental and theoretical studies on the atmospheric degradation of 1, 1, 2, 2, 3, 3, 4-heptafluorocyclopentane. *Atmos. Environ.* **2018**, *196*, 38−43.

(51) Staroverov, V. N.; Scuseria, G. E.; Tao, J.; Perdew, J. P. Comparative assessment of a new nonempirical density functional: Molecules and hydrogen-bonded complexes. *J. Chem. Phys.* **2003**, *119*, 12129−12137.

(52) Lee, C.; Yang, W.; Parr, R. G. Density-functional exchange-energy approximation with correct asymptotic behavior. *Phys. Rev. B* **1988**, *37*, 785−789.

(53) Tentscher, P. R.; Arey, J. S. Geometries and vibrational frequencies of small radicals: Performance of coupled cluster and more approximate methods. *J. Chem. Theory Comput.* **2012**, *8*, 2165−2179.

(54) Adamo, C.; Barone, V. Toward reliable density functional methods without adjustable parameters: The PBE0 model. *J. Chem. Phys.* **1999**, *110*, 6158−6170.

(55) Zhao, Y.; Truhlar, D. G. The M06 suite of density functionals for main group thermochemistry, thermochemical kinetics, non-covalent interactions, excited states, and transition elements: Two new functionals and systematic testing of four M06- class functionals and 12 other functionals. *Theor. Chem. Acc.* **2008**, *120*, 215−241.

(56) Stefan, V.; Kieron, B. Quantifying and Understanding Errors in Molecular Geometries. *J. Phys. Chem. Lett.* **2020**, *11*, 9957−9964.

(57) Éric, B.; Marika, S.; Neil, Q. S.; Ángel, J. P.-J.; Xu, X.; Juan, C. S.-G.; Carlo, A. Benchmarking Density Functionals on Structural Parameters of Small−/Medium-Sized Organic Molecules. *J. Chem. Theory Comput.* **2016**, *12*, 459−465.

(58) Jensen, F. Segmented Contracted Basis Sets Optimized for Nuclear Magnetic Shielding. *J. Chem. Theory Comput.* **2015**, *11*, 132−138.

(59) Oliveira, M. T. D.; Alves, J. M. A.; Braga, A. A. C.; Wilson, D. J. D.; Barboza, C. A. Do Double-Hybrid Exchange-Correlation Functionals Provide Accurate Chemical Shifts? A Benchmark Assessment for Proton NMR. *J. Chem. Theory Comput.* **2021**, *17*, 6876−6885.

(60) Flaig, D.; Maurer, M.; Hanni, M.; Braunger, K.; Kick, L.; Thubauvile, M.; Ochsenfeld, C. Benchmarking Hydrogen and Carbon NMR Chemical Shifts at HF, DFT, and MP2 Levels. *J. Chem. Theory Comput.* **2014**, *10*, 572−578.

(61) Teale, A. M.; Lutnæs, O. B.; Helgaker, T.; Tozer, D. J.; Gauss, J. Benchmarking density-functional theory calculations of NMR shielding constants and spin-rotation constants using accurate coupled-cluster calculations. *J. Chem. Phys.* **2013**, *138*, No. 024111.

(62) Zhang, C. P. *Investigation on synthesis of 1H, 1H, 2H-heptafluorocyclopentane*; Beijing Institute of Technology: Beijing, 2017.

(63) Tri, N. N.; Hailu, Y. M.; Van Duong, L.; Nguyen, M. T. Influence of Fluorination on Energetic Parameters of Silole, Phosphole, Thiophene, Oligomers of Silole and Related Acenes. *J. Fluorine Chem.* **2020**, *240*, No. 109665.

(64) Koopmans, T. Über die Zuordnung von Wellenfunktionen und Eigenwerten zu den Einzelnen Elektronen Eines Atoms. *Physica* **1934**, *1*, 104−113.

(65) Luo, J.; Xue, Z. Q.; Liu, W. M.; Wu, J. L.; Yang, Z. Q. Koopmans' Theorem for Large Molecular Systems within Density Functional Theory. *J. Phys. Chem. A* **2006**, *110*, 12005−12009.

(66) Politzer, P.; Murray, J. S. The electrostatic potential as a guide to molecular interactive behavior. In *Chemical Reactivity Theory: A Density Functional View*; Chattaraj, P. K., Ed.; CRC Press: Boca Raton, 2009.

(67) Murray, J. S.; Politzer, P. Electrostatic potentials: chemical applications. In *Encyclopedia of Computational Chemistry*; Schleyer, P. V. R., Ed.; John Wiley & Sons: West Sussex, 1998; pp 912.

(68) Murray, J. S.; Politzer, P. The electrostatic potential: an overview. *WIREs Comput. Mol. Sci.* **2011**, *1*, 153−163.

(69) Lu, T.; Chen, F. W. Quantitative analysis of molecular surface based on improved Marching Tetrahedra algorithm. *J. Mol. Graphics Modell.* **2012**, *38*, 314−323.

(70) Lu, T.; Chen, Q. X. van der Waals Potential: An Important Complement to Molecular Electrostatic Potential in Studying Intermolecular Interactions. *J. Mol. Model.* **2020**, *26*, 315.

(71) Rappe, A. K.; Casewit, C. J.; Colwell, K. S.; Goddard, W. A.; Skiff, W. M. UFF, a full periodic table force field for molecular

mechanics and molecular dynamics simulations. *J. Am. Chem. Soc.* **1992**, *114*, 10024−10035.

(72) Grimme, S.; Hansen, A.; Brandenburg, J. G.; Bannwarth, C. Dispersion-corrected mean-field electronic structure methods. *Chem. Rev.* **2016**, *116*, 5105−5154.

(73) Lu, T.; Chen, Q. Interaction Region Indicator (IRI): A Simple Real Space Function Clearly Revealing Both Chemical Bonds and Weak Interactions. *Chem. Methods* **2021**, *1*, 231−239.

(74) Skodje, R. T.; Truhlar, D. G. Parabolic tunneling calculations. *J. Phys. Chem.* **1981**, *85*, 624−628.

(75) Calvert, J. G.; Derwent, R. G.; Orlando, J. J.; Tyndall, G. S.; Wallington, T. J. *Mechanisms of Atmospheric Oxidation of the Alkanes*; Oxford University Press: Oxford, U.K., 2008.

(76) Xie, Y.; Schaefer, H. F.; Cotton, F. A. The radical anions and the electron affinities of perfluorinated benzene, naphthalene and anthracene. *Chem. Commun.* **2003**, 102−103.

(77) Rienstra-Kiracofe, J. C.; Tschumper, G. S.; Schaefer, H. F.; Sreela, N.; Ellison, G. B. Atomic and Molecular Electron Affinities: Photoelectron Experiments and Theoretical Computations. *Chem. Rev.* **2002**, *102*, 231−282.

(78) Lu, T.; Chen, F. Bond order analysis based on the Laplacian of electron density in fuzzy overlap space. *J. Phys. Chem. A* **2013**, *117*, 3100−3108.

(79) Reed, A. E.; Curtiss, L. A.; Weinhold, F. Intermolecular interactions from a natural bond orbital, donor-acceptor viewpoint. *Chem. Rev.* **1988**, *88*, 899−926.

(80) Klod, S.; Kleinpeter, E. Ab initio calculation of the anisotropy effect of multiple bonds and the ring current effect of arenes-application in conformational and configurational analysis. *J. Chem. Soc, Perkin Trans. 2* **2001**, *2*, 1893−1898.

(81) Schleyer, P. V. R.; Maerker, C.; Dransfeld, A.; Jiao, H.; van Eikema Hommes, N. J. R. Nucleus-independent chemical shifts: a simple and efficient aromaticity probe. *J. Am. Chem. Soc.* **1996**, *118*, 6317−6318.

(82) Schleyer, P. V. R.; Jiao, H. What is aromaticity? *Pure Appl. Chem.* **1996**, *68*, 209.

(83) Becke, A. D.; Edgecombe, K. E. A simple measure of electron localization in atomic and molecular systems. *J. Chem. Phys.* **1990**, *92*, 5397−5403.